IEEE Access
Multidisciplinary : Rapid Review : Open Access Journal

Received January 13, 2020, accepted January 22, 2020, date of publication February 7, 2020, date of current version February 18, 2020.

Digital Object Identifier 10.1109/ACCESS.2020.2972269

Fraction-Order Total Variation Image Blind Restoration Based on Self-Similarity Features

LUOYU ZHOU [1,2], TAO ZHANG [3], YUMENG TIAN [1], AND HU HUANG [1]

[1]Electronics and Information School, Yangtze University, Jingzhou 434023, China
[2]National Demonstration Center for Experimental Electrical and Electronic Education, Yangtze University, Jingzhou 434023, China
[3]Quality Engineering and Smart Technology Research Centre, Brunel University London, Uxbridge UB8 3PH, U.K.

Corresponding author: Luoyu Zhou (luoyuzh@yangtzeu.edu.cn)

This work was supported in part by the Hubei Provincial Natural Science Foundation of China under Grant 2019CFB233, and in part by the National Natural Science Foundation of China under Grant 61901059.

ABSTRACT To improve the artifacts of the restoration results restored by existing blind restoration method, an effective image blind restoration method using self-similarity as prior information is proposed for restoring the blurry images. Firstly, the fraction-order model is achieved by extending integer-order total variation, which is prone to reduce artifacts. Motivated by the fact that the introduction of prior information is beneficial to improve the restoration results, we found that natural images usually exhibit some texture features. Self-similarity is a popular texture features and well-defined in the statistics. Therefore, this texture feature is introduced as prior information for the restoration model and further improving the restoration results. Finally, the cost function is generated and solved by semi-quadratic regularization. Experiments on various natural images showed that the proposed method can improve the performance relative to other image blind restoration algorithms in terms of both subjective vision and objective evaluation. The subjective analysis revealed that the proposed algorithm resulted in improved translation and improved artifact appearance. The objective evaluation showed that the proposed algorithm showed the best evaluation values, including Structural Similarity and Peak Signal-to-noise ratio. The restoration results of various images reveal that the proposed method is practical and effective in image restoration.

INDEX TERMS Image blind restoration, texture features, fraction-order total variation, prior information.

I. INTRODUCTION

Images are usually degenerated during the process of acquisition. Image degeneration is usually described as

$$g = f * k + n \tag{1}$$

where f is the sharp image, g is the blurry image, k is the blur kernel and n is additive noise. The purpose of blind restoration is to obtain a deblurring image from an observed image blurred by unknown blur kernel. The restoration processing is usually ill-posed due to the lack of prior information about sharp image and blur kernel. Therefore, it is necessary to add some regularization constraints or prior information on blurry images and blur kernels. Total variation (TV) regularization is a classical regularization term widely used in image inversion. It is proposed in [1] by Rudin et al. and shown as

$$\min_{u,k} J(u,k) = \frac{1}{2}\|k*u-g\|^2_{L^2(\Omega)} + \int_\Omega |\nabla u|\, dxdy \tag{2}$$

where u is the restoration image. Then, the blind restoration model is proposed in [2], shown as

$$\min_{u,k} J(u,k) = \frac{1}{2}\|k*u-g\|^2_{L^2(\Omega)} + \alpha_1 \int_\Omega |\nabla u|\, dxdy + \alpha_2 \int_\Omega |\nabla k|\, dxdy \tag{3}$$

$$|\nabla u| = \sqrt{(D_x u)^2 + (D_y u)^2}\quad |\nabla k| = \sqrt{(D_x k)^2 + (D_y k)^2} \tag{4}$$

where $|\nabla \cdot|$ denotes TV. In recent years, TV model has been improved by many scholars in [2]–[6]. Chen R et al. proposed a high-order regularization term for aerial image blind

The associate editor coordinating the review of this manuscript and approving it for publication was Muhammad Sharif.

restoration in [4]. Zhou L et al. proposed a fraction-order TV image blind restoration method in [5]. However, in these methods, there is no other prior information apart from TV regularization terms, and thus the restoration results still need to be improved.

In early stage, the blind restoration methods are mainly proposed based on prior information about edge-prediction strategies. However, the prediction seldom performs well without strong edges in observed images [7]–[9]. To avoid the edge prediction problem, some blind restoration methods propose to adopt different prior information, including L0 gradients [10], [11], directional filters [12] and sparsity [13]–[15]. However, similar to edge prediction, these prior information can be still improved. Therefore, it is of great interest to introduce appropriate prior information to improve the restoration results.

Motivated by the importance of prior information, we propose to use a texture feature of natural images as prior information. Then we build a fraction-order total variation blind restoration model based on this prior information. However, it is not easy to optimize the blind restoration model with some non-linear terms, such as fraction-order total variation and the other prior information. So we make use of the semi-quadratic regularization to optimize the model. Experimental results confirm that our method can achieve excellent restoration results.

This paper is organized as follows. Section II extracts an appropriate texture feature of natural images and introduces it as prior information. Section III describes the optimization of model. The experimental design and results are shown in Section IV and conclusion is displayed in Section V.

II. BLIND RESTORATION MODEL BASED ON PRIOR INFORMATION

A. FRACTION-ORDER TOTAL VARIATION

Fraction-order TV is proposed by extending integer-order TV. It is firstly applied in image denoising and obtains excellent denosing results. Motivated by successful application in denoising, it is applied in image blind restoration to achieve details and suppress the artificial edges simultaneously [5], shown as

$$\min_{u,k} J(u,k) = \left\|k^{*}u-g\right\|_{L^1(\Omega)}+\alpha_1\left\|\nabla^r u\right\|_{L^1(\Omega)}+\alpha_2\left\|\nabla^r k\right\|_{L^1(\Omega)} \tag{5}$$

where ∇^r represents r-order (r is a decimal). The model has significantly improved the restoration results. However, the lack of prior information leads to poor robustness. Therefore, we introduce the prior information as a new regularization term. Then the model is updated as follows

$$\min_{u,k} J(u,k) = \|k*u-g\|_{L^1(\Omega_x)}+\alpha_1\left\|\nabla^r u\right\|_{L^1(\Omega)} +\alpha_2\|lk\|^2_{L^2(\Omega)}+\lambda\rho(u) \tag{6}$$

where l is Laplacian operator. In this paper, Laplacian operator is used as the regularization term for blur kernel, because it is better for estimating smooth blur kernel. α_1, α_2 and λ are the parameters for balancing all terms. $\rho(u)$ is the prior information term, which is described in detail next.

B. PRIOR INFORMATION FOR BLIND RESTORATION

Extraction of prior information has been studied in recent years [16], [17]. Natural images usually exhibit heavy-tail distributions, described as various statistical models, such as generalized normal distribution [18], GSM model [19], self-similarity [20]. Self-similarity is a popular feature for image textures and is well-defined in the statistics. It is defined as

$$B_H(at) = |a|^H B_H(t) \tag{7}$$

where $B_H(at)$ is the H-dependent random process, H is the Hurst parameter, a is the scale parameter. This equality shows that the output distribution is relevant to the scale parameter and Hurst parameter.

The Hurst parameter reflects the fractal of images. Therefore, some scholars use the Hurst parameter to analyze natural images [21], [22]. Fractional Brownian Motion (FBM), also proposed in [20], is a usual random process exhibiting self-similarity. Actually, image details are easily contaminated by noise and blur during image acquisition and image transmission. However, existing blind restoration methods usually restore the edges excessively, because it will regard the fine details as noise and clear them from the images. In recent years, it is found that FBM is credible prior information for fine details and has been applied successfully in image denosing [22] and image super-resolution [23].

However, we find that the application of FBM in the form of prior information encounters some difficulties. Firstly, it has to compute inversion of a large matrix. Furthermore, Hurst parameter may vary with the variation of coordinates. Therefore, we use a patch-based FBM as prior information of image. The inversion of matrix can be easily solved because image patch size is limited. Besides, Hurst parameter is constant in the interior of patch and varies throughout different patches, which is accordant with practical image features. Therefore, the prior information for blind restoration is defined as

$$\rho(u) = \sigma_N^2\left(u^T \sum\nolimits_{i,H}^{-1} u\right) \tag{8}$$

where u denotes the restoration image, $\sum_{i,H}$ denotes a patch-based FBM covariance matrix with Hurst parameter H and patch i, σ_N^2 denotes noise variation of the observed blurry image. It is estimated by existing noise estimation algorithms [24]. The estimation of the Hurst parameter is shown in [22]. Considering computational complexity, the size of patch are set as 64×64. Then, the proposed blind restoration model is shown as

$$\min_{u,k} J(u,k) = \|k*u-g\|_{L^1(\Omega_x)}+\alpha_1\left\|\nabla^r u\right\|_{L^1(\Omega)} +\alpha_2\|lk\|^2_{L^2(\Omega)}+\lambda\sigma_N^2\left(u^T \sum\nolimits_{i,H}^{-1} u\right) \tag{9}$$

Next, we will aim to solve the optimization of the proposed model (9).

III. OPTIMIZATION OF THE PROPOSED MODEL

The optimization of the proposed method can been solved by iterative minimization methods. However, existing methods can only obtain the approximate solution [25], [26], because of non-convex L1-norm and non-linear prior information. To tackle them, the model (9) is transformed into model (10) by introducing two relaxation factors.

$$\begin{aligned}\min_{w,z,u,k} J(w;z;u;k) = &\left(\|z\|_{L^1} + \frac{\beta_1}{2}\|z-(k*u-g)\|_{L^2}^2\right)\\ &+\alpha_1\left(\|w\|_{L^1} + \frac{\beta_2}{2}\left\|w-\nabla^r u\right\|_{L^2}^2\right)\\ &+\alpha_2\|lk\|_{L^2}^2 + \lambda\sigma_N^2\left(u^T \sum\nolimits_{i,H}^{-1} u\right)\\ &\text{where } \beta_1,\beta_2\to\infty \end{aligned}\tag{10}$$

where β_1 and β_2 are the introduced coefficients, w and z are the introduced relaxation factors. When $\beta_1, \beta_2 \to \infty$, the model (10) is equivalent to the model (9). Then we will obtain the solution of model (10) by extreme value theory of partial differential equations. The minimization sequence of all variables is shown as

$$w \to z \to u \to k \tag{11}$$

A. OPTIMIZATION OF RELAXATION FACTORS

Firstly, we solve the relaxation factor w by fixing the other variables and optimizing

$$\min_w \alpha_1\left(\|w\|_{L^1} + \frac{\beta_2}{2}\left\|w-\nabla^r u\right\|_{L^2}^2\right)\tag{12}$$

The solution of w is achieved by setting the partial derivative of model (12) to w as 0 and shown as

$$w^{n+1} = \max\left\{\left\|\nabla^r u^n\right\| - 1/\beta_2\right\}\frac{\nabla^r u^n}{\|\nabla^r u^n\|}\tag{13}$$

where n denotes iteration index. Then the update for z is obtained by repeating the same procedure,

$$z^{n+1} = \max\left\{\left\|k^n * u^n - g\right\| - 1/\beta_1\right\}\frac{k^n * u^n - g}{\|k^n * u^n - g\|}\tag{14}$$

B. OPTIMIZATION OF RESTORATION IMAGES

The restoration image u is solved by fixing the other variables and optimizing

$$\begin{aligned}\min_u \left(\frac{\beta_1}{2}\|z-(k*u-g)\|_{L^2}^2\right) + \alpha_1\left(\frac{\beta_2}{2}\left\|w-\nabla^r u\right\|_{L^2}^2\right)\\ +\lambda\sigma_N^2\left(u^T\sum\nolimits_{i,H}^{-1} u\right)\end{aligned}\tag{15}$$

The partial derivative of model (15) to u is set as 0 and shown as

$$\begin{aligned}&\beta_1\tilde{k}*(k*u-g-z)\\ &\quad+\alpha_1\beta_2\tilde{\nabla}^r\left(\nabla^r u - w\right) + \lambda\sigma_N^2\sum\nolimits_{i,H}^{-1} u = 0\end{aligned}\tag{16}$$

where $\tilde{k} = k(-x,-y)$ and $\tilde{\nabla}^r = \nabla^r_{-x,-y}$

Due to non-linearity, the solution of (16) can be achieved by gradient descent.

$$\begin{aligned}\frac{u_{t+1}-u_t}{\Delta t} \approx \frac{\partial u}{\partial t} = \beta_1\tilde{k}*(k*u-g-z)\\ +\alpha_1\beta_2\tilde{\nabla}^r(\nabla^r u - w) + \lambda\sigma_N^2\sum\nolimits_{i,H}^{-1} u\end{aligned}\tag{17}$$

Then, we obtain its equivalent gradient descent flow

$$\begin{aligned}u_{t+1} = u_t + \beta_1\Delta t\tilde{k}*(k*u_t-g-z)\\ +\alpha_1\beta_2\Delta t\tilde{\nabla}^r(\nabla^r u_t - w) + \lambda\Delta t\sigma_N^2\sum\nolimits_{i,H}^{-1} u_t\end{aligned}\tag{18}$$

The restoration image u converges slowly with time evolution and the stopping criteria is shown as

$$\delta_t = \frac{\|u_{t+1}-u_t\|}{\|u_t\|} \le \delta \tag{19}$$

where δ is stopping threshold. On each iteration, δ_t is calculated. If $\delta_t \le \delta$ meets, the gradient descent flow will stop.

C. OPTIMIZATION OF BLUR KERNEL

Finally, by fixing the other variables, the optimization of k is shown as

$$\min_h \frac{\beta_1}{2}\|z-(k*u-g)\|_{L^2}^2 + \alpha_2\|lk\|_{L^2}^2 \tag{20}$$

Then, the partial derivative of model (20) to k is set as 0 and shown as

$$\frac{\beta_1}{2\alpha_2}\tilde{u}\,(k*u-g-z) + \tilde{l}lk = 0 \tag{21}$$

Equation (21) can be successfully solved by Fast Fourier Transform, that is

$$\frac{\beta_1}{2\alpha_2}U^{\#}(UK-G-Z) + L^{\#}LK = 0 \tag{22}$$

where # denotes complex conjugate. Therefore, the solution of blur kernel is achieved as

$$k^{n+1} = F^{-1}\left[\frac{\beta_1(U^{n+1})^{\#}(G+Z^{n+1})}{\beta_1\left|U^{n+1}\right|^2 + 2\alpha_2|L|^2}\right]\tag{23}$$

where U, G, Z, L are Fourier transform of u, g, z, l; F^{-1} denotes inverse Fourier transform.

The solution of the model (10) can be achieved by iteratively calculating w, z, u, k. The restoration results will be presented in Section IV.

D. IMPLEMENTATION DETAILS

The initial value for u^0 is chosen to be the observed image as it is the good approximation of u. The initial value for blur kernel k^0 is chosen to be the delta function $\delta(x,y)$. The initial size of blur kernel is critical, because the blind restoration is ill-posed and it will take much time for convergence. Similar to other classical blind restoration method, the initial size of blur kernel is set as 51 × 51. We stop the iteration when the relative variation of cost function is less than 10^{-4} or the number of iterations exceeds 2000.

(a) Original images (left: boat, middle: monarch, right: lighthouse)

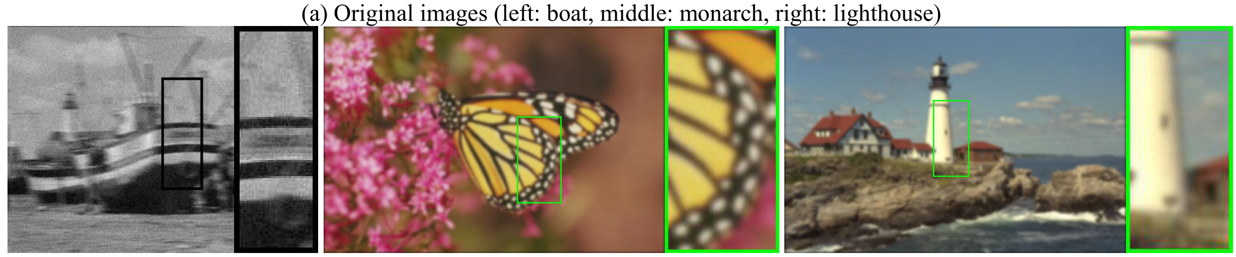

(b) Blurry images

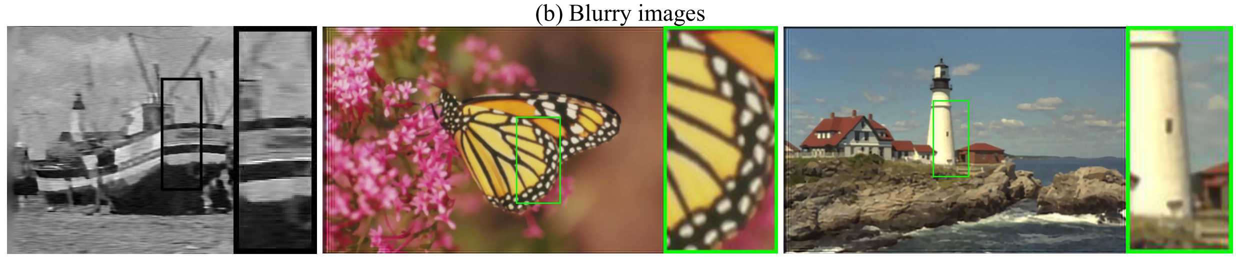

(c) The restoration images by Zhong L et al.

(d) The restoration images by Zhou L et al.

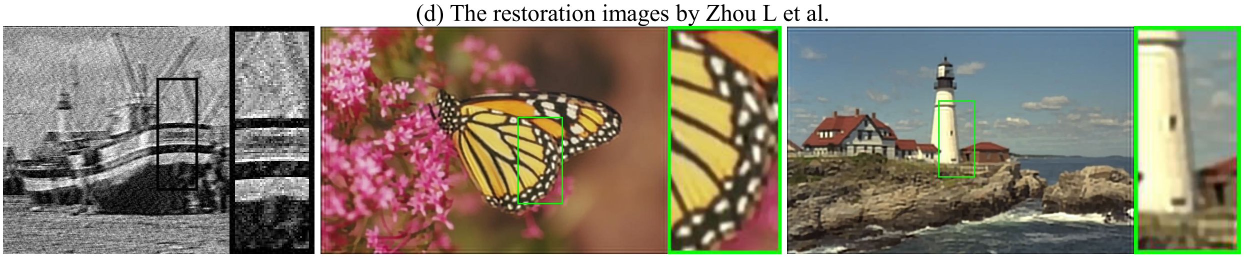

(e) The restoration images by Elmi S Y et al.

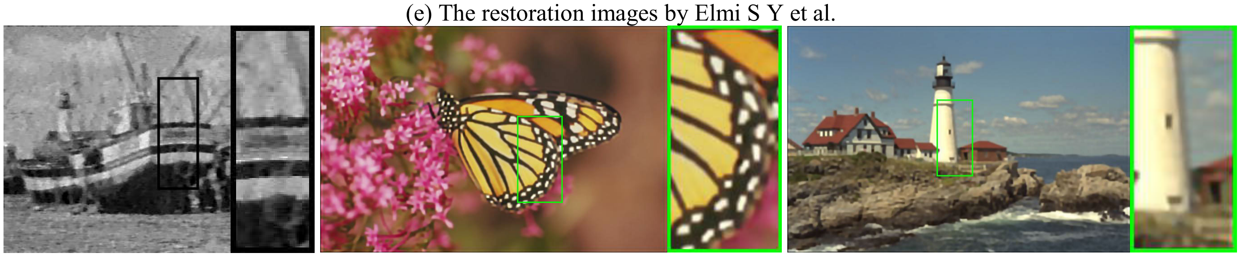

(f) The restoration images by our proposed method

FIGURE 1. Blind restoration results of synthetic blurry images.

As discussed in section III, when $\beta_1, \beta_2 \to \infty$, model (10) is equivalent to model (9). However, it will take shorter time to run the method with smaller β_1 and β_2. So they are set as a geometrical sequence, ranging from 1 to 10^7. Additionally, the common ratio of the proposed geometrical sequence is set as 3.

The parameters α_1 and α_2 in blind restoration model are positive parameters which measure the tradeoff between a

TABLE 1. The performance indicators of structural similarity (SSIM) and peak signal-to-noise ratio (PSNR) in Figure 1.

	Noise variance σ^2	SSIM/PSNR			
		Zhong L et al.	Zhou L et al.	Elmi S Y et al.	Proposed
Boat	50	0.3519/16.99	0.5294/21.30	0.2839/17.98	**0.6245/23.65**
Monarch	0	0.8355/17.48	0.9147/21.71	0.9458/25.08	**0.9552/26.11**
Lighthouse	0	0.6479/18.96	0.7787/22.58	0.7924/23.51	**0.8037/24.02**

(a) Blurry image (b) [Zhong L et al.] (c) [Zhou L et al.] (d) [Elmi S Y et al.] (e) Our result

FIGURE 2. Blind restoration results of Hollywood.

good fit and regularity of the solution of u and h. α_1 smooth the noise and is inversely proportional to the image noise. On the other hand, the parameter $\alpha 2$ controls the spread of the PSF and is set as 1.4. The parameter λ measures the weight of texture features and is set as 0.25. The decimal order r is a critical parameter in fraction-order TV model, which is determined experimentally and set as 1.5 in this paper.

IV. EXPERIMENTAL RESULTS

To comprehensively testify the restoration performance, we test a large number of blurry images, including synthetic blurry images and real blurry images, which are respectively shown in Section IV.A and Section IV.B. Then, we discuss the running time and convergence in Section IV.C.

Moreover, to show the superiority of our proposed method, we also present the restoration results of other restoration methods, which are shown as follows.

1. Zhong L et al. proposed the blind restoration method in [12] which is based on inverse radon transform and directional filters.

2. Zhou L et al. proposed the blind restoration method in [5] which is based on fraction-order variation with no prior.

3. Elmi S Y et al. proposed the blind restoration method in [11] which is based on multi-resolution ringing removal.

A. BLIND RESTORATION FOR SYNTHETIC IMAGES

In the sub-section, the grayscale image (boat), as shown in Fig.1(a)-left, is blurred by a motion blur kernel function. The color images (monarch and lighthouse), as shown in Fig.1(a)-middle and Fig.1(a)-right, are downloaded from LIVE Public-Domain Subjective Image Quality Database [27]. The blurry images and the restoration images are shown in Fig.1(b)~(f) respectively. It is found that the proposed algorithm is generally superior to the other algorithms in terms of visual effect, especially in augmented details. We also compare the proposed algorithm with three other algorithms based on two performance indicators, including Structural Similarity Index Measure (SSIM) and Peak Signal-to-Noise Ratio (PSNR), which are respectively shown in (24) and (25).

$$\mathrm{SSIM} = \frac{(2\mu_u\mu_f + c_1)(2\sigma_{uf} + c_2)}{(\mu_u^2 + \mu_f^2 + c_1)(\sigma_u^2 + \sigma_f^2 + c_2)} \tag{24}$$

$$\mathrm{PSNR} = 10\log_{10}\left[\frac{255 \times 255 \times M \times N}{||u-f||_2^2}\right] \tag{25}$$

where u and f represent the original image and restored images μ and σ^2 represent the mean and variance of the image, σ_{xy} represent the covariance of the image, M $\times$ N is the size of image.

As shown in Table 1, the proposed algorithm is generally superior to the competitive algorithms, especially for the noise image (boat). When the noise level is low, the performance indicators of Elmi S Y are the second-best. However, when the noise level is high, the performance indicators of Zhong L and Elmi S Y are poor. Anyway, our proposed algorithm is the best among these algorithms in terms of SSIM and PSNR.

B. BLIND RESTORATION FOR REAL IMAGES

In the sub-section, we test our algorithm on various real images. All images are restored by using these blind restoration algorithms, including Zhong *et al.* [12], Zhou and Tang [5], Elmi *et al.* [11] and our proposed algorithm.

Firstly, the image, ''Hollywood'', and its restoration results are shown in Fig.2. In general, all restoration results exhibit sharper image details compared with the blurry image. However, it is seen from the enlarged red rectangle that the result

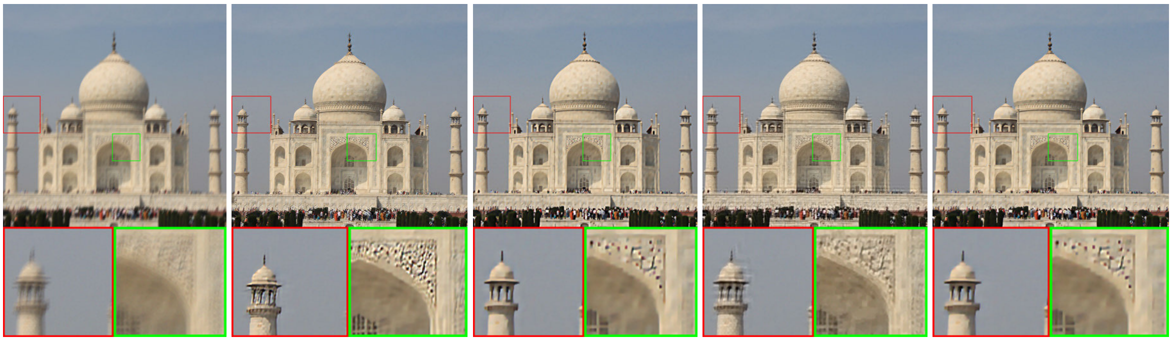

(a) Blurry image (b) [Zhong L et al.] (c) [Zhou L et al.] (d) [Elmi S Y et al.] (e) Our result

FIGURE 3. Blind restoration results of Church.

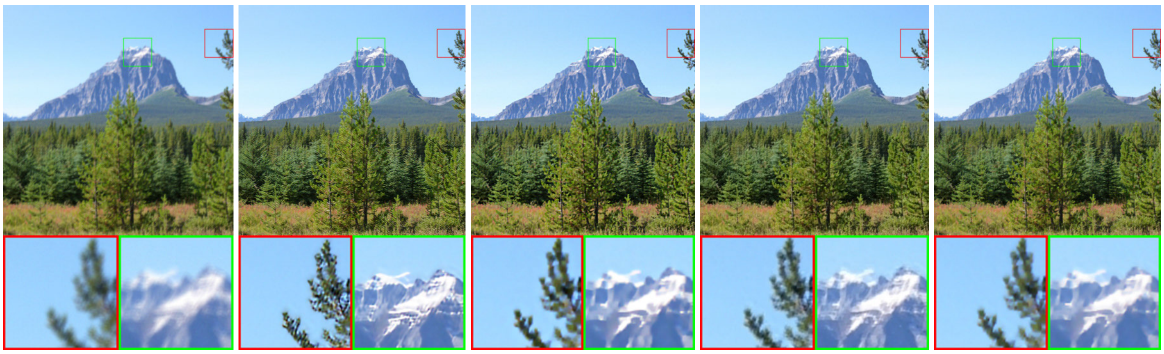

(a) Blurry image (b) [Zhong L et al.] (c) [Zhou L et al.] (d) [Elmi S Y et al.] (e) Our result

FIGURE 4. Blind restoration results of Hill.

TABLE 2. The running time of the restoration algorithms.

	Running time (unit: Sec)			
	Zhong L et al.	Zhou L et al.	Elmi S Y et al.	Proposed
Hollywood (Fig.2)	278.15	247.27	302.68	306.19
Church (Fig.3)	166.02	134.54	176.51	190.17
Hill (Fig.4)	194.16	173.18	211.52	229.86
Lyndsey (Fig.5)	342.47	405.25	383.28	564.88

of Zhong L et al. (Fig.2(b)) has the largest translation (the width of pillars) among these restoration results. In addition, from the enlarged green rectangle, there are some ringing artifacts around letter "S" in Fig.2(b) and Fig.2(d), but the colored lights in Fig.2(b) exhibit clearer. Even in Fig.2(c), the letter "S" is distorted and the colored lights are still blurry. It is obvious that our result (Fig.2(e)) exhibits sharper image details (e.g., the colored lights) and fewer artifacts (e.g., the ringing artifacts around the letter "S").

The restoration results of the other examples are all shown in Fig.3∼Fig.5, including Church, Hill and Lyndsey. These images are obtained from the classical image database [28]. In particular, the images are blurred by unknown and different blur kernels, which is challenging for blind restoration. However, it is found that our results exhibit sharper details and fewer ringing artifacts compared with the other methods.

Finally, two more challenging blurry images are respectively displayed in Fig.6 and Fig.7. Fig.6 exhibits the restoration images on a Text image. Our method achieves clearer letters and fewer ringing artifacts than the other blind restoration methods. What is more, the poor result of Zhou L et al. (Fig.6(c)) shows that the algorithm does not converge to optimal solution. Fig.7 exhibits the restoration results on an ultrasonic logging image. It is obvious that our method achieves more details with clearer fractures.

C. THE RUNNING TIME AND CONVERGENCE ANALYSIS

The proposed method is optimized by semi-quadratic regularization and gradient descent method, and thus the method is time-consuming. Actually improving the image quality as well as reducing the running time is a challenge problem for blind restoration. Table 2 shows the running time of processing Fig.2∼Fig.5 by these blind restoration algorithms. These blind restoration algorithms are implemented on MATLAB. It is noted that we do not focus on the running time of the algorithm. Actually, the code can be further optimized by working with C++ instead of MATLAB or using parallel algorithms.

In addition, the prior information is introduced into the fraction-order total variation model for blind restoration and

(a) Blurry image (b) [Zhong L et al.] (c) [Zhou L et al.] (d) [Elmi S Y et al.] (e) Our result

FIGURE 5. Blind restoration results of Lyndsey.

(a) Blurry image (b) [Zhong L et al.] (c) [Zhou L et al.] (d) [Elmi S Y et al.] (e) Our result

FIGURE 6. Blind restoration results of text image.

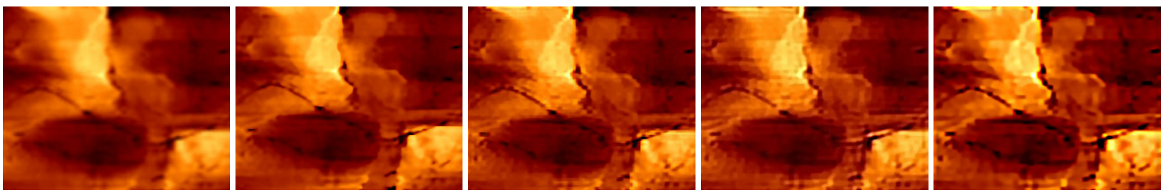

(a) Blurry image (b) [Zhong L et al.] (c) [Zhou L et al.] (d) [Elmi S Y et al.] (e) Our result

FIGURE 7. Blind restoration results of ultrasonic logging image.

FIGURE 8. Ground truth data: 4 images and 8 blur kernels, resulting in 32 test images.

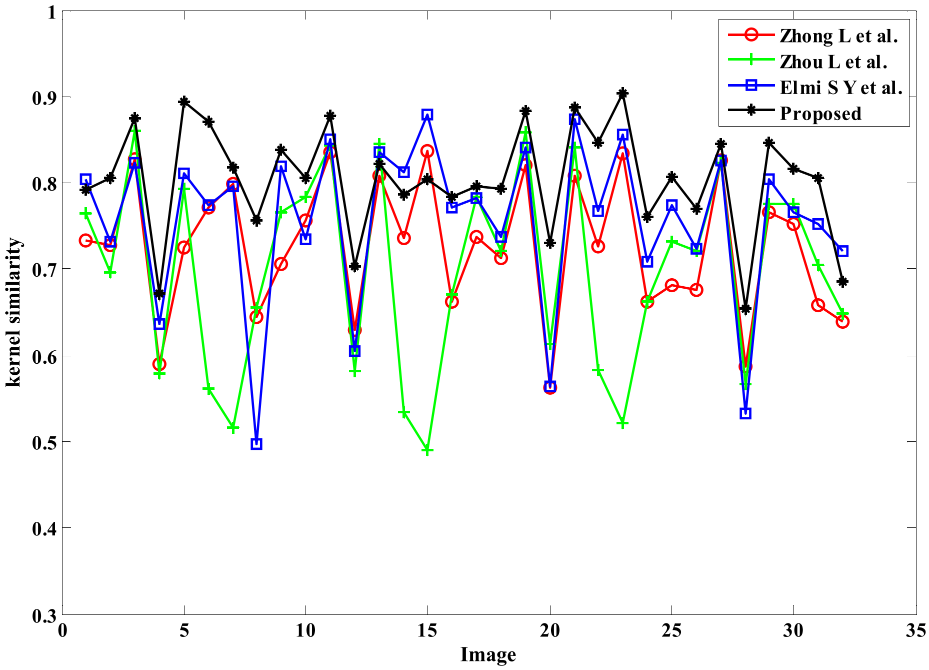

FIGURE 9. The kernel similarity for comparing convergence of the blind restoration methods.

thus the proposed method converges well. We quantitatively evaluate convergence by the kernel similarity. The kernel similarity $S(h, k)$ is proposed in [29] and shown as

$$S(h, k) = \max_{\gamma} \frac{\sum_{\tau} h(\tau) \cdot k(\tau + \gamma)}{||h||_2 \cdot ||k||_2} \tag{26}$$

where h is the known blur kernel, k is the estimated blur kernel, τ is element coordinates, γ is the possible shift between the two kernels. All images are achieved from the dataset of Levin in [30] and [31], including 32 blurry images generated by 4 images and 8 blur kernels. Fig.8 illustrates that the proposed method convergences well.

V. DISCUSSION AND CONCLUSION

A new image blind restoration method has been proposed to sharpen the edges and reduce ringing artifacts. In this paper, we firstly propose a blind restoration model based on fraction-order TV. Then, our algorithm introduces self-similarity as prior information to improve the restoration effect and convergence property. Application of the algorithm to test images resulted in restored images with reduced artifacts, improved edge sharpness, and improved translation. Our proposed method outperforms existing methods in terms of both visual quality and objective evaluation

The limitation of this work is that the parameters are determined experimentally by different test. Actually, these parameters rely on the image features, including blur, noise and so on. In addition, the blur in our paper are all spatially invariant blur. Some spatially variant blurs can be transformed into the spatially invariant blur by nonlinear transformation. They will be discussed and studied in the future work.

REFERENCES

[1] L. I. Rudin, S. Osher, and E. Fatemi, "Nonlinear total variation based noise removal algorithms," *Phys. D, Nonlinear Phenomena*, vol. 60, nos. 1–4, pp. 259–268, Nov. 1992.

[2] T. Chan and C.-K. Wong, "Total variation blind deconvolution," *IEEE Trans. Image Process.*, vol. 7, no. 3, pp. 370–375, Mar. 1998.

[3] K. Shao, Y. Zou, Y. Liu, C. Li, and B. Fu, "Based on total variation regularization iterative blind image restoration algorithm," *Sensors Transducers*, vol. 167, no. 3, pp. 36–42, 2014.

[4] R. Chen, H. Jia, X. Xie, and W. Gao, "Blind restoration for nonuniform aerial images using nonlocal Retinex model and shearlet-based higher-order regularization," *J. Electron. Imaging*, vol. 26, no. 3, May 2017, Art. no. 033016.

[5] L. Zhou and J. Tang, "Fraction-order total variation blind image restoration based on L1-norm," *Appl. Math. Model.*, vol. 51, pp. 469–476, Nov. 2017.

[6] L. Yan, H. Fang, and S. Zhong, "Blind image deconvolution with spatially adaptive total variation regularization," *Opt. Lett.*, vol. 37, no. 14, p. 2778, Jul. 2012.

[7] O. Shacham, O. Haik, and Y. Yitzhaky, "Blind restoration of atmospherically degraded images by automatic best step-edge detection," *Pattern Recognit. Lett.*, vol. 28, no. 15, pp. 2094–2103, Nov. 2007.

[8] H. Shen, W. Zhao, Q. Yuan, and L. Zhang, "Blind restoration of remote sensing images by a combination of automatic knife-edge detection and alternating minimization," *Remote Sens.*, vol. 6, no. 8, pp. 7491–7521, Aug. 2014.

[9] J. Dong, J. Pan, and Z. Su, "Blur kernel estimation via salient edges and low rank prior for blind image deblurring," *Signal Process., Image Commun.*, vol. 58, pp. 134–145, Oct. 2017.

[10] L. Xu, S. Zheng, and J. Jia, "Unnatural L0 sparse representation for natural image deblurring," in *Proc. IEEE Conf. Comput. Vis. Pattern Recognit.*, Jun. 2013, pp. 1107–1114.

[11] Y. Elmi Sola, F. Zargari, and A. M. Rahmani, "Blind image deblurring based on multi-resolution ringing removal," *Signal Process.*, vol. 154, pp. 250–259, Jan. 2019.

[12] L. Zhong, S. Cho, D. Metaxas, S. Paris, and J. Wang, "Handling Noise in Single Image Deblurring Using Directional Filters," in *Proc. IEEE Conf. Comput. Vis. Pattern Recognit.*, Jun. 2013, pp. 612–619.

[13] R. Fergus, B. Singh, A. Hertzmann, S. T. Roweis, and W. T. Freeman, "Removing camera shake from a single photograph," *ACM Trans. Graph.*, vol. 25, no. 3, p. 787, Jul. 2006.

[14] A. Ahmed and L. Demanet, "Leveraging diversity and sparsity in blind deconvolution," *IEEE Trans. Inf. Theory*, vol. 64, no. 6, pp. 3975–4000, Jun. 2018.

[15] C.-Y. Liu, C.-L. Yao, and J. Xiong, "Geophysical potential field anomaly separation method with optimal mother wavelet and spatial locating multiresolution analysis (MRA)," *IEEE Access*, vol. 7, pp. 62840–62851, 2019.

[16] A. Lee, D. Mumford, and J. Huang, "Occlusion models for natural images: A statistical study of a scale-invariant dead leaves model," *Int. J. Comput. Vis.*, vol. 41, nos. 1–2, pp. 35–59, 2001.

[17] P. Moulin and J. Liu, "Analysis of multiresolution image denoising schemes using generalized Gaussian and complexity priors," *IEEE Trans. Inf. Theory*, vol. 45, no. 3, pp. 909–919, Apr. 1999.

[18] E. Simoncelli and E. Adelson, "Noise removal via Bayesian wavelet coring," in *Proc. 3rd IEEE Int. Conf. Image Process.*, Lausanne, Switzerland, Dec. 2002, pp. 379–382.

[19] J. Portilla, V. Strela, M. Wainwright, and E. Simoncelli, "Image denoising using scale mixtures of Gaussians in the wavelet domain," *IEEE Trans. Image Process.*, vol. 12, no. 11, pp. 1338–1351, Nov. 2003.

[20] B. B. Mandelbrot and J. W. Van Ness, "Fractional Brownian motions, fractional noises and applications," *SIAM Rev.*, vol. 10, no. 4, pp. 422–437, Oct. 1968.

[21] B. Pesquet-Popescu and J. Vehel, "Stochastic fractal models for image processing," *IEEE Signal Process. Mag.*, vol. 19, no. 5, pp. 48–62, Sep. 2002.

[22] I. Zachevsky and Y. Y. J. Zeevi, "Statistics of natural stochastic textures and their application in image denoising," *IEEE Trans. Image Process.*, vol. 25, no. 5, pp. 2130–2145, May 2016.

[23] I. Zachevsky and Y. Y. Zeevi, "Single-image superresolution of natural stochastic textures based on fractional Brownian motion," *IEEE Trans. Image Process.*, vol. 23, no. 5, pp. 2096–2108, May 2014.

[24] L.-Y. Zhou and Z.-B. Zhang, "No-reference image quality assessment based on noise, blurring and blocking effect," *Optik*, vol. 125, no. 19, pp. 5677–5680, Oct. 2014.

[25] W. Zhang, Y. Cao, R. Zhang, and Y. Wang, "Image denoising using total variation model guided by steerable filter," *Math. Problems Eng.*, vol. 2014, pp. 1–11, Jan. 2014.

[26] G. Aubert and P. Kornprobst, "Mathematical problems in image processing: Partial differential equations and calculus of variations," *Appl. Intell.*, vol. 40, no. 2, pp. 291–304, 2006.

[27] LIVE. *Public-Domain Subjective Image Quality Database*. Accessed: 2006. [Online]. Available: http://live.ece.utexas.edu/research/quality/subjective.htm

[28] *Blurry Image Database*. Accessed: 2012. [Online]. Available: https://www.cse.huji.ac.il/~raananf/projects/deblur/results/

[29] H. Zhe and M. H. Yang, "Good regions to deblur," in *Proc. Eur. Conf. Comput. Vis.*, 2012, pp. 1–14.

[30] A. Levin, Y. Weiss, F. Durand, and W. T. Freeman, "Understanding and evaluating blind deconvolution algorithms," in *Proc. IEEE Conf. Comput. Vis. Pattern Recognit.*, Jun. 2009, pp. 1964–1971.

[31] *Ground Truth Data*. Accessed: 2009. [Online]. Available: https://www.wisdom.weizmann.ac.il/levina/papers/LevinEtalCVPR09Data.zip

LUOYU ZHOU received the B.S. degree in optical information science and technology from the University of Science and Technology of China (USTC), Hefei, China, in 2008, and the Ph.D. degree in optical engineering from the Changchun Institute of Optics, Fine Mechanics and Physics, Chinese Academy of Sciences, (CIOMP, CAS), Changchun, China, in 2013. He is currently a Lecturer with the School of Electronics and Information, Yangtze University, China. His current research interests include image processing, computer vision, and artificial intelligence.

TAO ZHANG received the B.E. degree in electronic science and technology from the University of Electronic Science and Technology of China (UESTC), Chengdu, China, in 2008, the M.E. degree in optical engineering from the Changchun Institute of Optics, Fine Mechanics and Physics, Chinese Academy of Sciences (CIOMP, CAS), Changchun, China, in 2011, and the Ph.D. degree in mechanical engineering from the University of Huddersfield, Huddersfield, U.K., in 2018. He is currently a Research Fellow with the Quality Engineering and Smart Technology Research Centre, Brunel University London. His current research interests include robotics, the Internet of Things (IoT), surface metrology, computer vision, and data analytics.

YUMENG TIAN received the B.S. degree in electronic information science and technology from Xi'an Technological University, Xi'an, China, in 2018. She is currently pursuing the M.E. degree with Yangtze University, Jingzhou, China. Her current research interests include image/video restoration, sparse representation, and image quality assessment.

HU HUANG received the B.S. degree in electronic information science and technology from Wuhan Polytechnic University, Wuhan, China, in 2019. He is currently pursuing the M.E. degree with Yangtze University, Jingzhou, China. His current research interests include image/video processing, high performance computing, and parallel computing.